

A Comparison of Gamma-Ray Detectors (CdTe, NaI:Tl & BGO) Using Radioisotope Sources

PHYC40870 - Space Detector Laboratory

Orlaith Ní Dhúill –

(Other Group Members*; Bruce Ritter, Flora Vyas & Eris Dempsey*)

Table of Contents

Introduction **1**
Background **2**
Background: The Detectors *2*
Background: The Radioisotopes *3*
Background: Gamma-Ray Spectra *3*
Experimental Methods & Set-up **3**
Data Collection Steps *3*
Data Analysis Steps *4*
Results **5**
Discussion of Results **5**
Applications **8**
Space Application *8*
General Application *9*
References **10**
Appendix **11**

Author's Note; *All group code and supporting tests are available in our shared repository at https://github.com/Bruce-A-R/High_Energy_Detector_Lab.git. Some aspects of the coding and background research were carried out with the help of AI based tools and reputable external resources such as StackOverflow.*

Abstract

This experiment examined the performance of three gamma ray detectors: CdTe, NaI(Tl), and BGO. Gamma ray spectra were collected using the MAESTRO system, and Gaussian fits were applied to the photopeaks to determine their centroids, widths, and areas. These fits were used to generate energy calibration curves, calculate the energy resolution across different energies, and determine both absolute and intrinsic efficiencies for each detector. The detectors were also tested at several off-axis angles to assess how their response changed with orientation. The results showed clear differences in resolution, detection efficiency, and angular sensitivity that reflected the underlying detector materials and operating principles. Based on these findings, the strengths and limitations of each detector type were evaluated in the context of high energy astrophysics and space-based instrumentation. Overall, the experiment provided a full comparison of CdTe, NaI(Tl), and BGO, and demonstrated how detector design influences gamma ray measurement under controlled laboratory conditions.

Introduction

Gamma-ray astronomy is space research regarding a range of the most energetic and extreme processes within the known universe, including topics such as studies of pulsars, GRBs, supernovae and black holes. Gamma-ray detection involves capturing high-energy photons within a range of about 10keV to hundreds of GeV. These photons generally contain data about non-thermal and relativistic processes that can't be observed at low energies. This process of data collection is different to optical or infrared observations, which rely on reflected or emitted light.

The detection of high-energy photons can involve many experimental challenges. This is because gamma rays cannot be focused by normally known optics, detection relies on interactions with denser materials through different processes (photoelectric effect**,** Compton scattering**,** pair production etc) specialised detectors convert these interactions into data signals.

The work reflected within this report discusses our group laboratory experiment whereby we calibrated and characterised three detectors (CdTe, NaI:Tl and BGO), measuring their energy resolution, efficiency and off-axis response to assess their suitability for different space missions.

Background

The Detectors

In this experiment, 3 types of detectors were used and compared:

- Cadmium Telluride (CdTe) solid-state detector
- Two scintillator detectors;
    - Thallium-doped Sodium Iodide (NaI:Tl)
    - Bismuth Germanate (BGO).

These detectors are used quite a lot in space-based gamma ray research because they provide good energy resolution and reliable operating efficiency that make them suitable for high energy measurements.

Specific Detector Details:

At a glance;
CdTe is well suited for compact missions that require good low energy resolution., NaI(Tl) provides high light yield and is commonly used in all sky monitors. BGO is used when strong stopping power at higher energies is required.

- ***CdTe Detector***;
  This is a direct bandgap semiconductor that directly converts absorbed gamma-ray energy into electron-hole pairs which are proportional to photon energy. Under applied voltage, charges are collected at the electrode which generates a current that can be measured, digitised and saved.

- ***NaI:Tl & BGO Detectors;***
  These two detectors are scintillation detectors; which means that they re-emit some of the absorbed gamma-ray energy as visible light. This emitted visible light is then detected and amplified using a photomultiplier tube (PMT) to produce an electrical signal. Each detector type has their own advantages regarding energy resolution, efficiency, and suitability for specific mission profiles. Na(TI) detectors are well known for their high light yield and fair costs, while CdTe detectors are great in energy resolution and because they are compact.



Figures 1. CAD Model of the BGO|630V detector.

The Radioisotopes

Background: Gamma-Ray Spectra

The detectors interact with the high-energy photons in different ways.

- The Photoelectric Effect
- Compton Scattering & Continuum
- Escape peaks
- Pair Production

When combined, they produce complex spectra by a monochromatic source, emitting photons of single energy. '*Appendix Figure 1'*, displays a perfect example of the three interactions of high-energy photons with a detector. In practice, unless the source is very active or the detector takes a very long time to process each γ-ray event, pile-up happens so rarely that the spectrum falls off rapidly beyond the photopeak.

Experimental Methods & Set-up

Radiation Safety – Mentioned in PHYC40870 Handbook

Although these sources are all low intensity sources, we were cautious when handling through specific safety measures.

- *Sources were handled and used only with the explicit permission of the lab instructor, who signed them in and out*
- *Plastic tweezers were used in our handling of the sources both for personal and the protection of the sources. We ensured that the sources were carefully handled without damaging the centre.*
- *We did not have food nor drink in the laboratory.*

This experiment is based on comparing the three different detectors. Identifying similarities, differences, strength and weaknesses of all three detectors. Each detector had to be calibrated first to identify the energy response. The performance of each detector was found by determining;

- Energy resolution as a function of energy
- Absolute and intrinsic efficiencies as functions of energy
- Off-axis performance of the detector

Data Collection Steps

The three detectors were set up such that data was collected directly using the (MAESTRO Multichannel Analyzer Emulation Software, n.d.)[1] application on the laboratory computers. This software is An MCA "emulation" software package which is compatible with gamma and alpha spectroscopy systems. The detection provided data files in the format of '.mca ' for the CdTe and '.spe' for the NaI and BGO detectors. The three detectors had essentially the same setup in terms of steps taken to acquire the data. All sources were positioned at set distances of 16cm for the Na(TI), 15cm for the BGO and 10cm from the CdTe detector. Acquisition times of each sources and detector was consistently set to 200s observation. The angles explored were also consistent at 0°, 45°, 90° and 135° for each detector and source. We were also sure to acquire standard background observation for each isotope at an angle of 0° for buffer deduction within results.

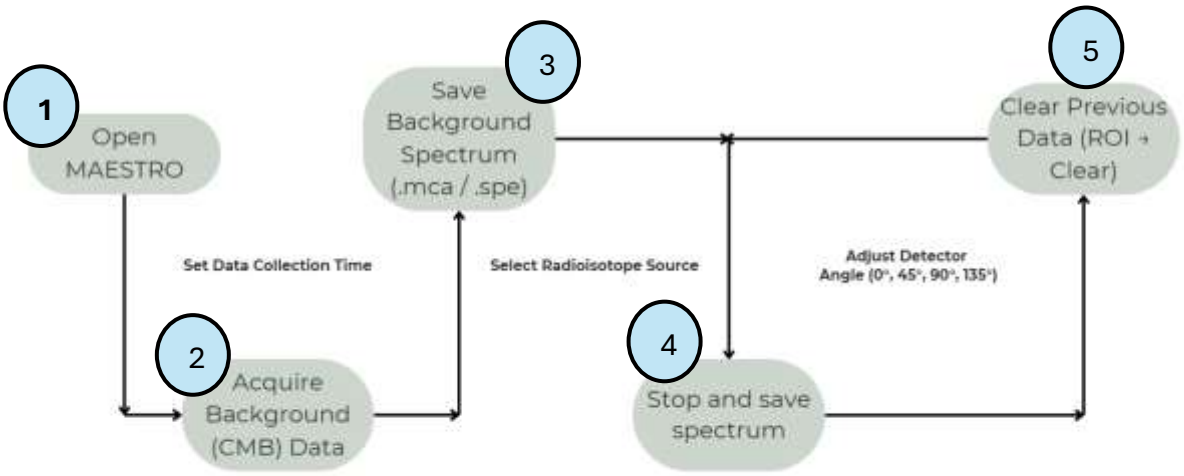

Figure 2. General experimental steps taken to obtain raw data.

Once collected, the detection data was analysed by fitting the data models to spectra. This was completed by fitting the parametric model to photopeaks. An example of a raw MAESTRO spectrum is shown in '*Appendix Figure 2'*.

Data Analysis Steps

To analyse the data, parametric peak models were fitted to spectra, this was helpful in determining parameters such as line position, width & area, which in turn were useful in calibration and characterisation Some necessary equations which were considered during the code building processes are outlined below;

1. ***Gaussian Curve***

   To analyse the spectra, each photopeak was modelled with a Gaussian line shape, which provided the peak position, width, and area needed for calibration and characterization. The Gaussian function used to construct this code is found in '*Eq 1*' below.

$$f(x;\mu,\sigma^2,A) = \frac{A}{\sigma\sqrt{2\pi}}\exp\left(-\frac{(x-\mu)^2}{2\sigma^2}\right) \qquad \textit{(Eq 1)}$$

2. ***Calibration curve (channel to energy conversion)***

   The Spectral data obtained from the detector system were imported into python for analysis. Each file was parsed to reconstruct the full gamma-ray spectrum and plotted for visual interpretation. Then Gaussian functions *(Eq 1)* were then fitted to the prominent peaks corresponding to known radioisotope energies. Using the plots produced, the photopeak channel number shows a calibration curve. The calibration curve was linear and had the form of an equation. By correlating the channel number of these fitted peak centroids with their established photon energies, an energy calibration curve was generated.

$$E = c_1 \times channel + c_0 \qquad \textit{(Eq 2)}$$

3. ***Energy resolution***

   The energy resolution for measuring how well the detector resolves two separate peaks that are close in energy levels were calibrated using the resolution (*Eq 3*) below, where 'δE' is the FWHM of the peak. The resolution at lower energies was approximated using (*Eq 3.1*)

$$R = \left(\frac{\delta E}{E}\right) \qquad \textit{(Eq 3)}$$

$$R^2 = \alpha E^{-2} + bE^{-1} + c \qquad \textit{(Eq 3.1)}$$

4. ***Absolute and Intrinsic Efficiency***

The efficiency characterisation of the detector was performed by analysing spectral data from multiple radioactive sources. The following equations (*Eq 4-5*) were used to derive the efficiency as a function of energy.

$$\epsilon_{\text{Intrinsic}} = \frac{Count\ rate}{Rate\ of\ photon\ passing\ through\ detector} \qquad \textit{(Eq 4)}$$

$$\epsilon_{\text{Absolute}} = \frac{Count\ rate}{\text{Source Activity}} = G \times \epsilon_{\text{Intrinsic}} \qquad \textit{(Eq 4.1)}$$

Both efficiencies are related by geometric factor *'G'* (*Eq 4.2*). Here, '*A*' is the detector area and '*d*' is the source to detector distance.

$$G = \frac{A}{4\pi d^2} \qquad \textit{(Eq 4.2)}$$

The intrinsic peak efficiency was modelled using the empirical logarithmic relationship found in '*Eq 5'* below

$$ln\,\epsilon_p = a + b\,ln\,E + c(lnE)^2 \qquad \textit{(Eq 5)}$$

5. ***Characterisation of Off-Axis Response***

For calculating the off-axis response, we analysed data at angles of 0°, 45°, 90° and 135° degrees. As the photons in real life from astronomical sources are unlikely to be centered on-axis with the front of the detector in the moving spacecraft. This helped us in observing the off-axis performance of each detector.

Results

The data collected from the BGO, CdTe, and NaI(Tl) detectors using the MAESTRO application, all operated under nearly identical experimental conditions. This collected data was used to create plots for energy calibration, energy resolution as a function of energy, absolute and intrinsic efficiencies, and off-axis behaviour. Using the test and experiment code provided in our group GitHub repository (https://github.com/Bruce-A-R/High_Energy_Detector_Lab), the resulting spectra and plots showed that radioisotopes with longer half-lives, such as Am^{-241} and Cs^{-137} produced the most clearly defined peaks and the highest counts per second across all detectors. This, and all relevant resulting plots can be found in both within the Github repository and in the '*Appendix Figures'* which show background-subtracted spectra from the BGO detector for Am, Cs, Ba, and Co.

Linear energy calibration curves were made by fitting the channel positions of known photopeaks to their corresponding gamma-ray energies. All detectors produced a strong linear relationship, confirming stable electronic response. Among the three, the CdTe detector had the smallest slope in its energy to channel calibration, which shows minimal deviation at lower energies.

Energy resolution was evaluated by fitting Gaussian functions to the identified photopeaks in the calibration spectra. Each fit provided a centroid and FWHM, which were then used to calculate the energy resolution. From these results, the CdTe semiconductor detector provided the best resolution at low energies, while the NaI(Tl) and BGO detectors provided mostly medium-moderate resolution.

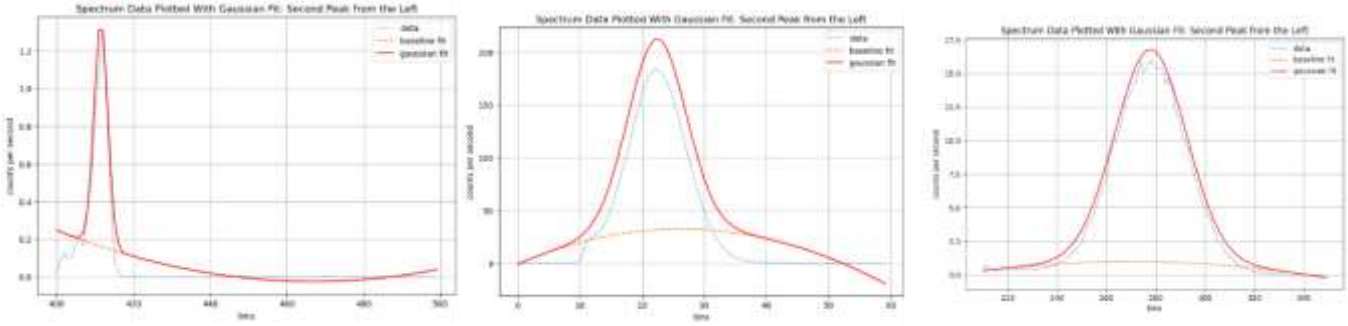

Figure 3. Gaussian peak fits across detectors. [From left to right; BGO, NaI(Tl), CdTe].

When comparing the detector peaks, the BGO peak shows lower amplitude and more noise, this is consistent with its low light yield. The NaI(Tl) peak is broader and smoother, which may reflect its moderate energy resolution. The CdTe peak is obviously way narrower and sharper, caused by the superior resolution of semiconductor detectors. Absolute and intrinsic efficiencies were calculated at the photon energies associated with each photopeak.

Detector	**Energy (min-max)**	**Count Rate**	**Absolute. Efficiency**	**Intrinsic Efficiency**	**Plot Outputs for Intrinsic Efficiency vs Energy**
CdTe	53.2	0.1	3e-6	1.66e-4	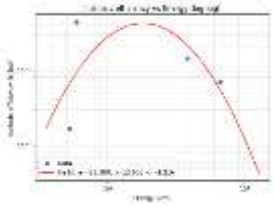
	661.7	0.4	11e-4	6.93e-4	
BGO	81.0	74.1	2e-3	0.128	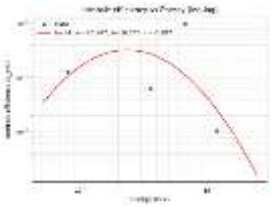
	1173.2	6	1.6e-4	0.010	
NaI(Tl)	59.5	519.9	0.014	0.900	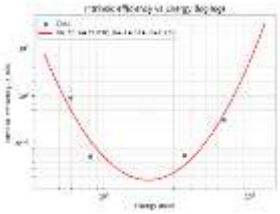
	661.7	180.7	4.8e-3	0.313	

Table 1. Summary of Data Results for each detector, Including 'Count Rate', both 'Absolute' and 'Intrinsic Efficiency', 'Energy Ranges' and plotted outputs for 'Intrinsic Efficiency vs Energy'.

From looking at the count rates and the shapes of the photopeaks, it's clear that each detector behaved differently in terms of efficiency. NaI(Tl) showed the highest absolute efficiency at the lower photon energies. This makes sense because NaI(Tl) has a large crystal volume, so there is a higher chance that incoming gamma photons will interact and be detected. BGO showed a moderate absolute efficiency overall, but it had a very high intrinsic efficiency at low energies. This reflects the strong stopping power of BGO, meaning that when photons do enter the crystal, they are very likely to be absorbed. CdTe had the

lowest absolute and intrinsic efficiencies because it has the smallest sensitive volume out of the three detectors. Even so, its semiconductor design still allowed it to pick out clear peaks, even when the count rate was low. Overall, the results showed how much detector material and positioning geometry influence efficiency, especially when comparing scintillators with a semiconductor detector.

The off-axis measurements also revealed that for all three detectors, the number of counts changed noticeably depending on the angle between the detector and the source. As the angle increased relative to the source, the count rate generally increased as well. Counts also increased as the distance between the detector and the source decreased. This shows that detector orientation and positioning play a large role in how many photons are actually detected.

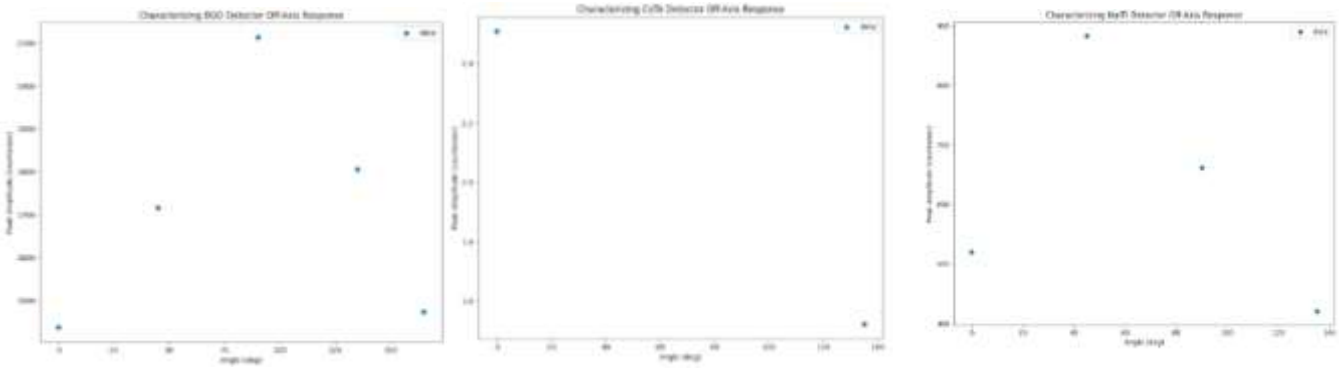

Figure 4. Off Axis Characterisation Output Plots.

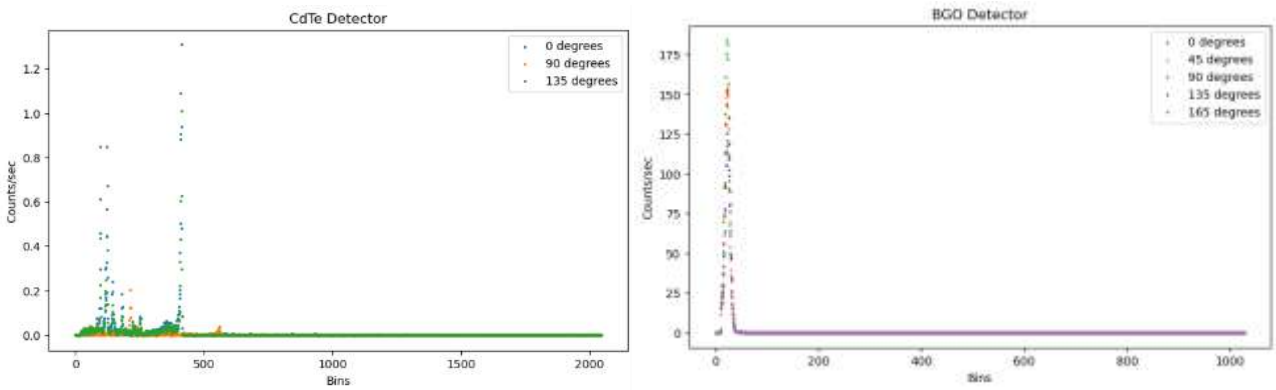

Figure 5. Plotted Output of Count Rate to Bin Number of both the CdTe and BGO detector respectively.

The angular measurements highlight how the detectors differ in their sensitivity as the orientation changes. For NaI(Tl), the peak amplitude is highest around 45 degrees and drops noticeably by 135 degrees. This behaviour is likely related to its crystal size and its relatively strong directional response. BGO shows a similar pattern, although its decline at larger angles is even steeper, which suggests that it is more sensitive to changes in orientation. For CdTe, we were only able to fit clear peaks at 0 degrees and 135 degrees. The peak amplitudes at 45 degrees and 90 degrees were too weak to produce reliable fits, probably because CdTe has a much smaller active volume and therefore a lower absolute count rate. Together, these results show that each detector responds differently to off-axis positioning and that geometry and material properties strongly influence angular sensitivity.

Discussion of Results

The results clearly show that the three detectors react differently across energy resolution, efficiency, and angular sensitivity. CdTe produced the narrowest and sharpest peaks, giving it the best resolution at low

energies. This comes from its semiconductor design and efficient charge collection. NaI(Tl) showed broader but smooth peaks, reflecting its decent resolution and reliable scintillation response. BGO made the lowest and noisiest peaks due to its low light yield, and weakest resolution of the three. These differences indicate that CdTe is best suited for precise low-energy spectroscopy, NaI(Tl) is best for general-purpose measurements, and BGO is most useful where high stopping power is more important than fine peak definition.

Efficiency trends also differed with energy. NaI(Tl) demonstrated the highest absolute efficiency at low energies because of its large crystal volume, which increases the likelihood of photon interactions. BGO showed moderate absolute efficiency but very high intrinsic efficiency at low energy, consistent with its strong gamma-ray stopping power. CdTe had the lowest absolute and intrinsic efficiencies due to its small active volume, that said it still produced clean peaks even at low count rates. These efficiency results follow the definitions outlined earlier, with absolute efficiency representing the probability of detecting an emitted photon and intrinsic efficiency representing the probability of detecting a photon that interacts with the detector. The activity decay corrections and energy-calibration references in the data analysis and appendix support our calculations.

The off-axis measurements showed a really clear angular dependence for all three detectors. NaI(Tl) showed its highest peak near 45° and an obvious decline by 135°, likely due to its crystal geometry and directional scintillation response. BGO displayed a similar pattern but with an even steeper drop-off at larger angles. CdTe's low count rate meant that only the 0° and 135° measurements produced reliable peaks, with the intermediate angles too weak to fit. These results show that orientation has a strong impact on detector response and that the degree of angular sensitivity varies with detector construction and volume.

Overall, the combined analysis of calibration behaviour, resolution trends, efficiency variations, and angular response allowed us to create a complete characterisation of each detector. NaI(Tl) is best for general spectroscopy where high efficiency and reasonable resolution are required. BGO is best for high-energy gamma detection and scenarios where high intrinsic efficiency and strong stopping power are needed. CdTe is the most suitable for precise low-energy analysis where sharp energy resolution is critical, despite its lower efficiency. Together, the results support the idea that the optimal detector depends heavily on the intended measurement conditions and mission requirements. In conclusion, these results clearly show that detector choice depends strongly on mission goals, energy range, and instrument geometry.

Note on Limitations of Detectors.

The ^{60}Co source activity was very low which limited the number of usable peaks. The CdTe detector produced no measurable signal at 90 degrees which restricted the off-axis analysis. Uncertainties were not fully propagated due to time constraints in developing the pipeline.

Applications

Space Applications

Gamma-ray detection is very useful for many different space applications. These detectors are useful for gamma-ray astronomy which is observation of high-energy emissions from cosmic sources like pulsars, supernovae, gamma-ray bursts, and active galactic nuclei. They also are used in spectroscopy of cosmic events, for finding composition and properties of space objects. Gamma-ray detectors are useful for monitoring cosmic rays and solar flare activity in space weather. Gamma ray detectors are also used in space engineering to test and check radioisotope power sources such as plutonium based RTGs during ground calibration., which power spacecraft, which is essential

for performance and safety. For planetary and lunar exploration missions, gamma-ray spectroscopy helps to understand the planetary composition of surfaces by detecting elements such as hydrogen and iron. Also, these detectors are useful for understanding dark matter annihilation and antimatter regions in space.

In space research right now, there are several missions actively use gamma-ray detection to support these applications. For high-energy astrophysics, the Fermi Gamma-ray Space Telescope, INTEGRAL, Swift, and AGILE observe gamma-ray bursts, pulsars, and active galactic nuclei. For planetary science, missions like Mars Odyssey, Lunar Prospector, MESSENGER, and Psyche use gamma-ray and neutron spectrometers to analyse planetary and asteroid compositions. SOHO and Solar Orbiter monitor solar events that produce high-energy particles. Lastly instruments like AMS-02 study antimatter and potential dark matter clues in space. These missions show how different detector materials are matched to specific science goals such as transient monitoring, planetary composition studies, and measurements of high energy particles

General Applications

Gamma ray detectors have a wide range of applications across medicine, industry, environmental monitoring, and scientific research. For example, BGO is widely used in medical PET scanners and in high energy physics calorimeters because these applications require strong gamma ray stopping power. Whereas CdTe detectors are widely used in compact gamma ray spectroscopy instruments because they operate at room temperature while still offering good energy resolution. CdTe is also used in X ray and gamma ray imaging panels for medical diagnostics and industrial inspection. NaI(Tl) is one of the most widely used scintillation detectors because it produces high light output, can be grown in large crystals, and is relatively inexpensive. It is used on large scale when it comes to SPECT cameras and for natural gamma logging tools in the oil and gas industry. These examples highlight how detector materials are chosen to match the required energy range, resolution, and practical constraints of each application

References

Detector Theory and Gamma Spectroscopy

1. Gilmore, G. (2008) *Practical Gamma-ray Spectrometry*. 2nd edn. Chichester: Wiley.
2. Knoll, G.F. (2010) *Radiation Detection and Measurement*. 4th edn. Hoboken, NJ: Wiley.
3. Mirion Technologies (n.d.) *Gamma-Ray Detection with Scintillators: Lab Experiment*. Available at: https://www.mirion.com.
4. Bissaldi, E. et al. (2009) 'Ground-based calibration and characterization of the Fermi Gamma-ray Burst Monitor detectors', *Experimental Astronomy*, 24(1–3), pp. 47–88. doi: 10.1007/s10686-008-9135-4.

Software and Laboratory Materials

5. PHYC40870 Space Detector Laboratory Handbook, Module teaching material.
6. ORTEC/AMETEK (n.d.) *MAESTRO Multichannel Analyzer Emulation Software*. Available at: https://www.ortec-online.com.

Gamma-ray Background and Physics

7. NASA (n.d.) *Gamma Rays*. NASA Science. Available at: https://science.nasa.gov/ems/12_gammarays/

Space Science / Detector Applications

8. NASA (n.d.) *Mars Odyssey: Science Instruments*. Available at: https://science.nasa.gov/mission/odyssey/science-instruments/.
9. Institute of High Energy Physics (n.d.) *Insight-HXMT Mission Overview*. Available at: http://hxmten.ihep.ac.cn/AboutHxmt.jhtml.

Appendix

All figures referenced in the main text are included here for clarity.

Isotope	Decay Mode	Half-Life	Energy/keV	Emission Fraction
^{60}Co	β	5.2714(5)	1173.228(3) 1332.492(4)	0.9985(3)
^{133}Ba	Electron Capture	10.537(3)	53.1622(6) 79.6142(12) 80.9979(11) 276.3989(12) 302.8508(5) 356.0129(7) 383.8485(12)	0.0214(3) 0.0265(5) 0.329(3) 0.0716(5) 0.1834(13) 0.6205(19) 0.0894(6)
^{137}Cs	β-	30.09(11)	661.657(3)	0.8499(20)
^{241}Am	α	432.2(6)	26.3446(2) 33.1963(3) 59.5409(1)	0.024(3) 0.00121(3) 0.3578(9)

Appen Table 1. Recreated based on Notebook; Properties for experimental radioisotopes; ^{60}Co, ^{133}Ba, ^{137}Cs and ^{241}Am

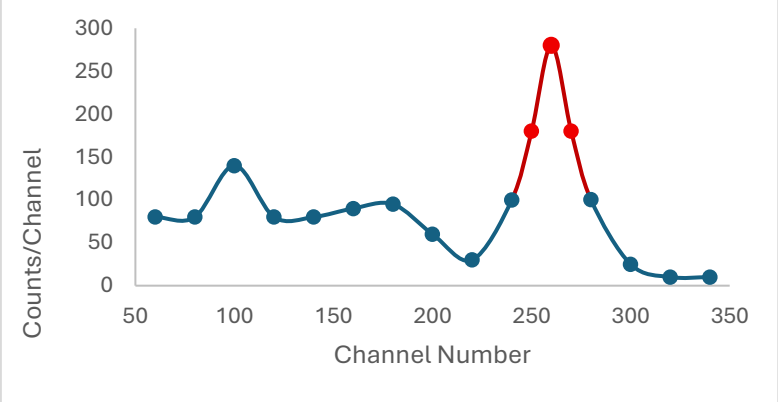

Appen Figure 1. Example Energy Spectrum of Photopeak of 137Cs Detection by Na:TI. Note the photopeak in red.

Plots outputs, from MAESTRO taken directly from lab.

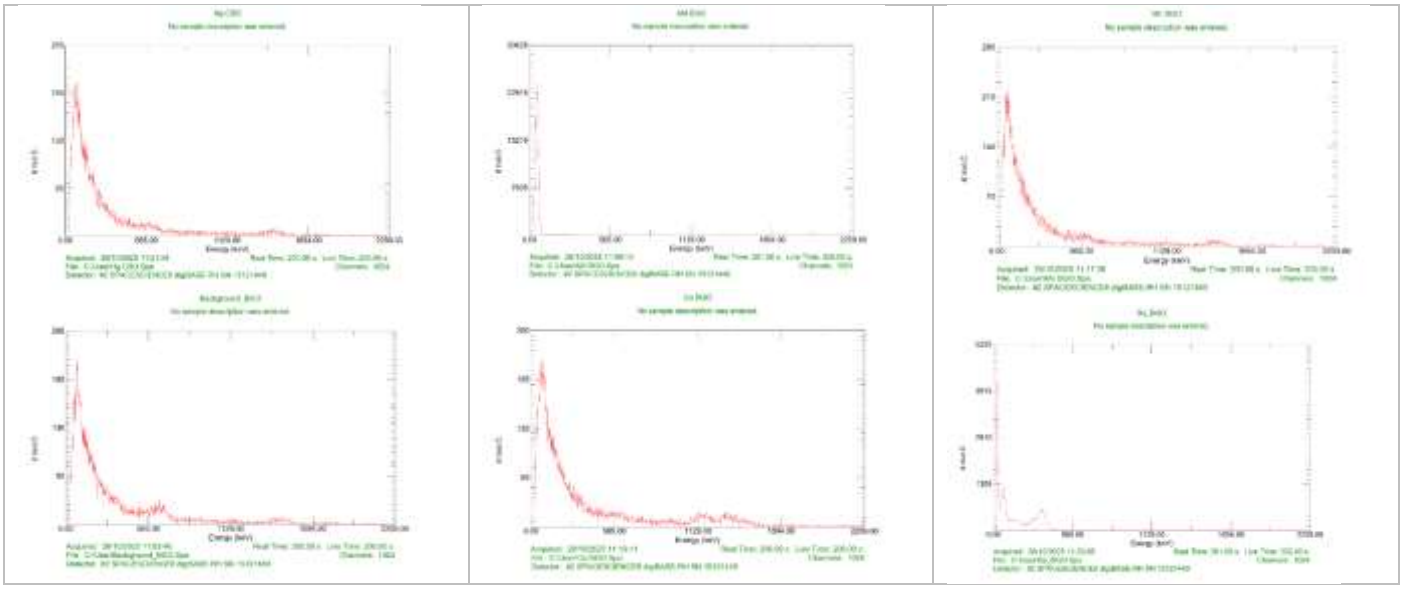

Appen. Figure 2. Plot Output Screenshots from the MAESTRO application.

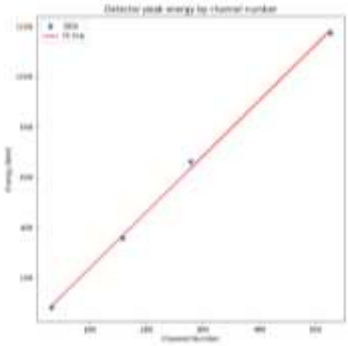

```
energy,peak loc,FWHM,amp,FWHM (keV)
80.9979,31.84227017642773,16.40337456521876,74.10169400769455,52.87585335249655
356.0129,157.61737677944632,21.239142945479472,35.96568596601065,63.617340130939674
1173.228,525.8389178162998,64.70050012122888,6.041577199899821,160.15620567754337
661.657,277.89419245189106,34.08759226804027,573.5945724977149,92.15705454016096
```

Appen. Figure 3.0 Plot & Results for Detector Peak Energy by Channel Number for BGO Detector.

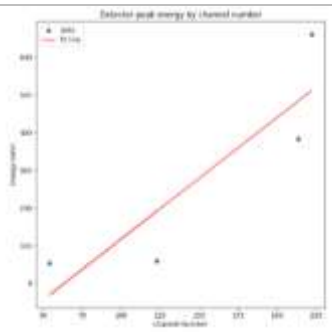

```
energy,peak loc,FWHM,amp,FWHM (keV)
59.5409,123.01482684760114,3.0485025787810005,2.5090444066272206,-194.90787236204733
53.1622,54.07762751209645,4.102194379595078,0.09560546591547849,-191.50838488561465
383.8485,213.5121303987218,4.633110714748646,0.8231751655758455,-189.79550885204043
661.657,222.23473685884932,4.605965116427936,0.3999513214481765,-189.88308770712902
```

Appen. Figure 3.1 Plot & Results for Detector Peak Energy by Channel Number for CdTe Detector.

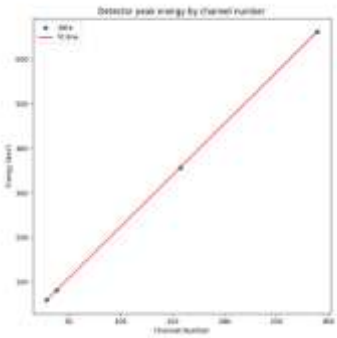

```
energy,peak loc,FWHM,amp,FWHM (keV)
59.5409,28.496875839888183,9.378679738246648,519.8545818412216,14.756419130811036
80.9979,38.15162244158822,10.366156644730012,30.094664817683096,17.03681302140009
356.0129,157.52791279683282,29.843763882148565,31.45339649196012,62.016717114226296
661.657,289.3165396009793,35.46625903525549,180.72601949288315,75.00082186931569
```

Appen. Figure 3.3 Plot & Results for Detector Peak Energy by Channel Number for the NaITi Detector.

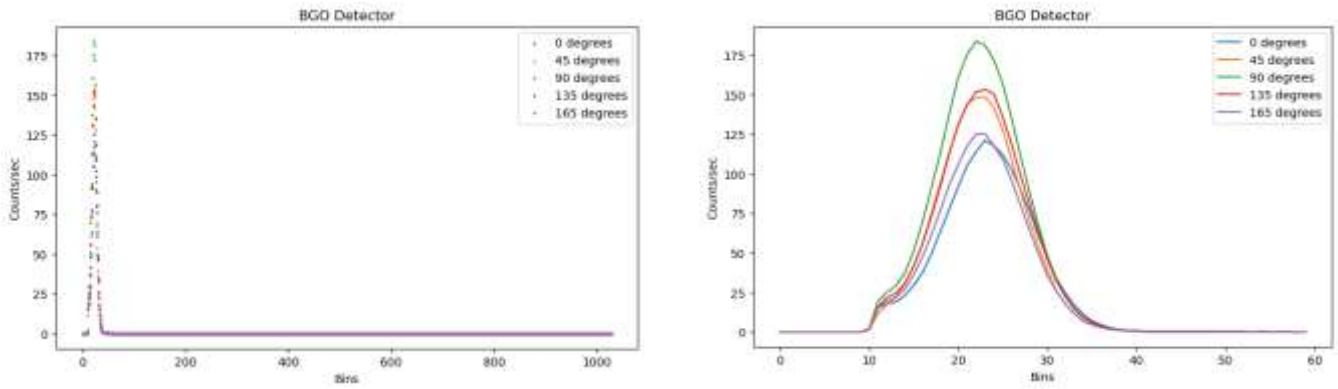

Appen Figure 5. Plotted Results for BGO detector Angular differences of Peak Data.

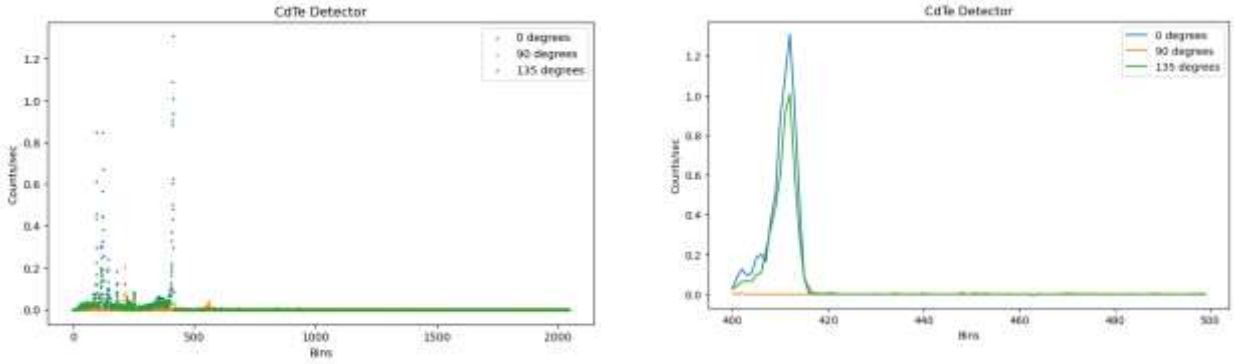

Appen Figure 6. Plotted Results for CdTe detector Angualr Differences of Peak Data.

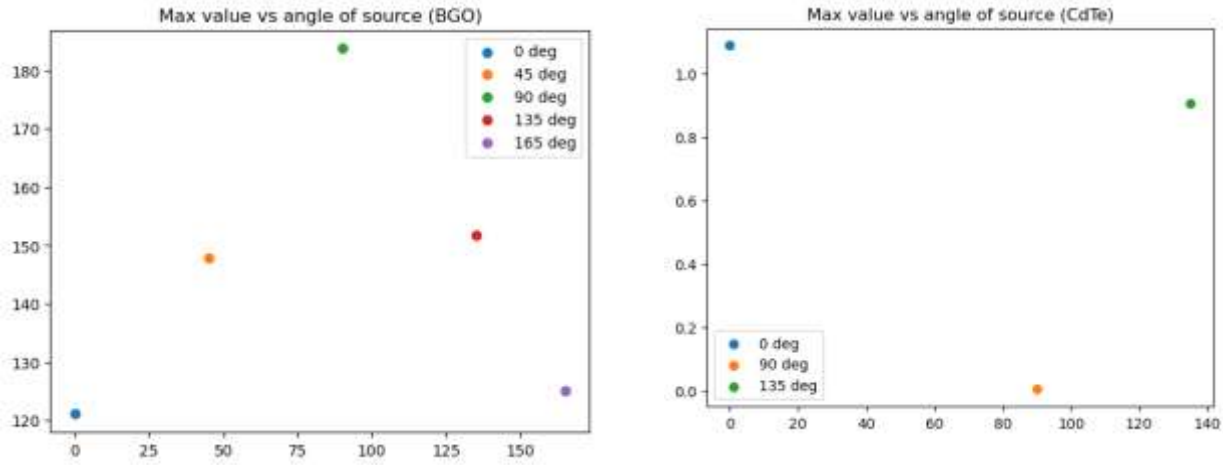

Appen Figure 7. Comparison of 'Max Value vs Angle of Source' for BGO & CdTe Data outputs.

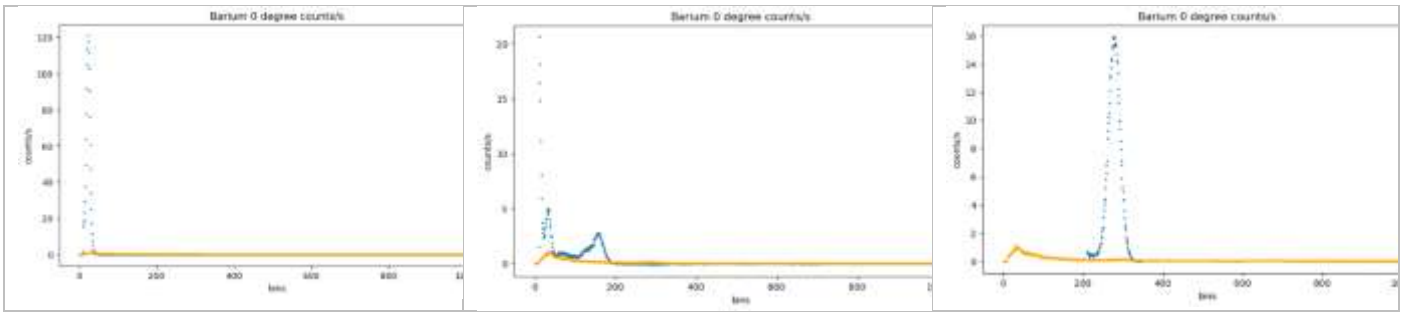

Appen Figure 8. Ba Plot outputs from testing

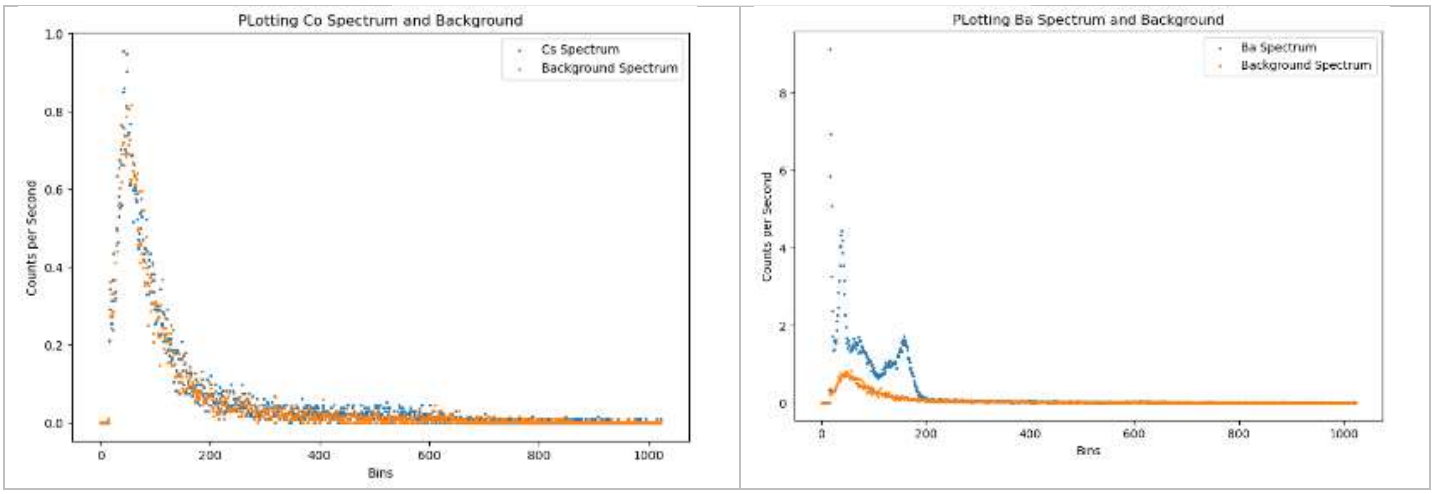

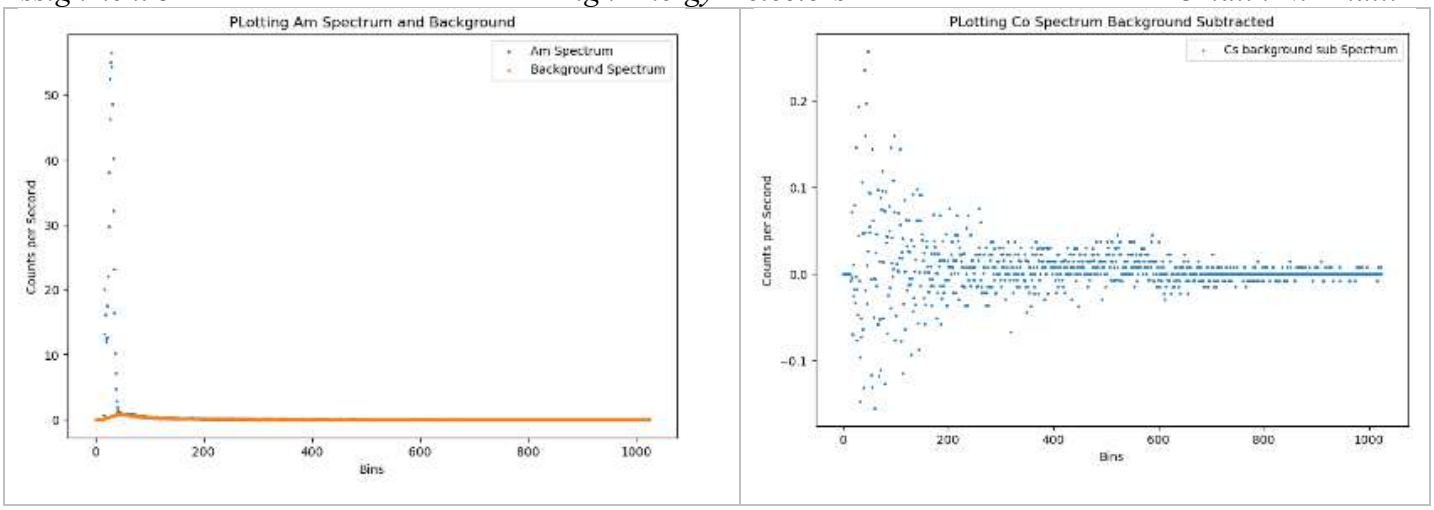

Appen Figure 9. All radioisotope plotted outputs for Spectrum & Background.

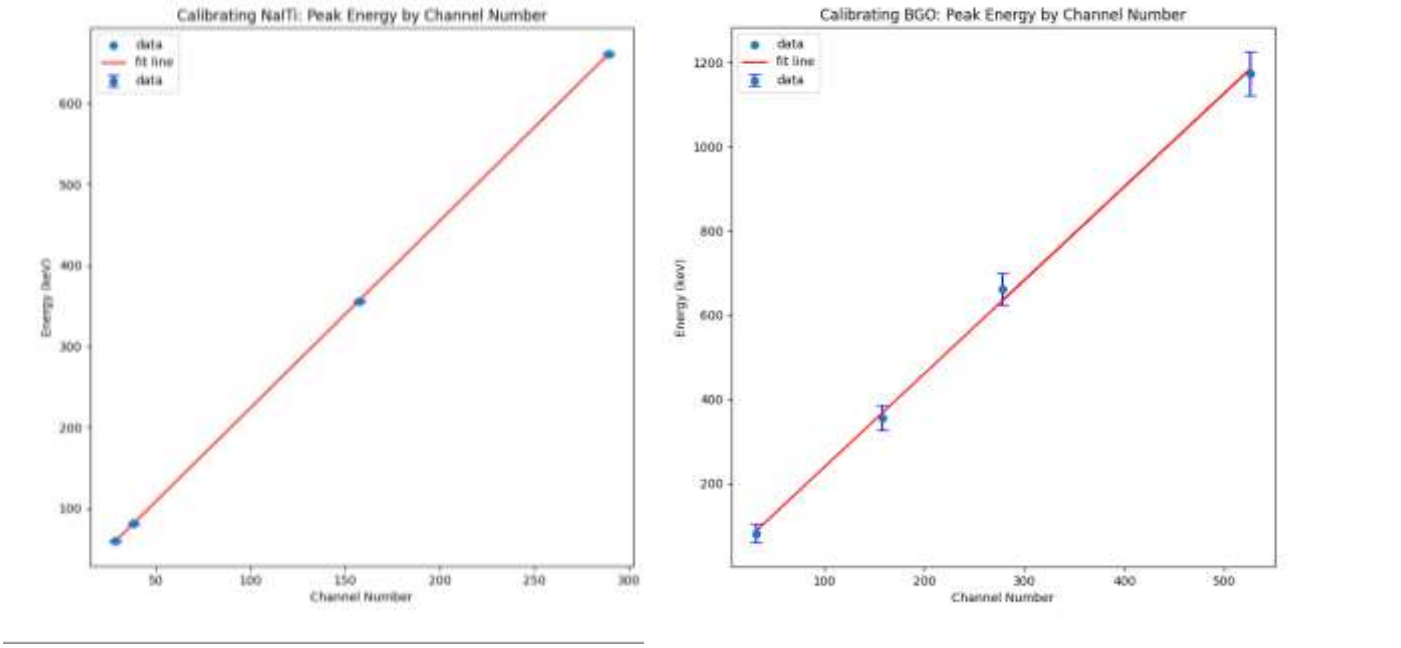

Appen Figure 10. Detector Calibration with and without error bars for channel numbers.

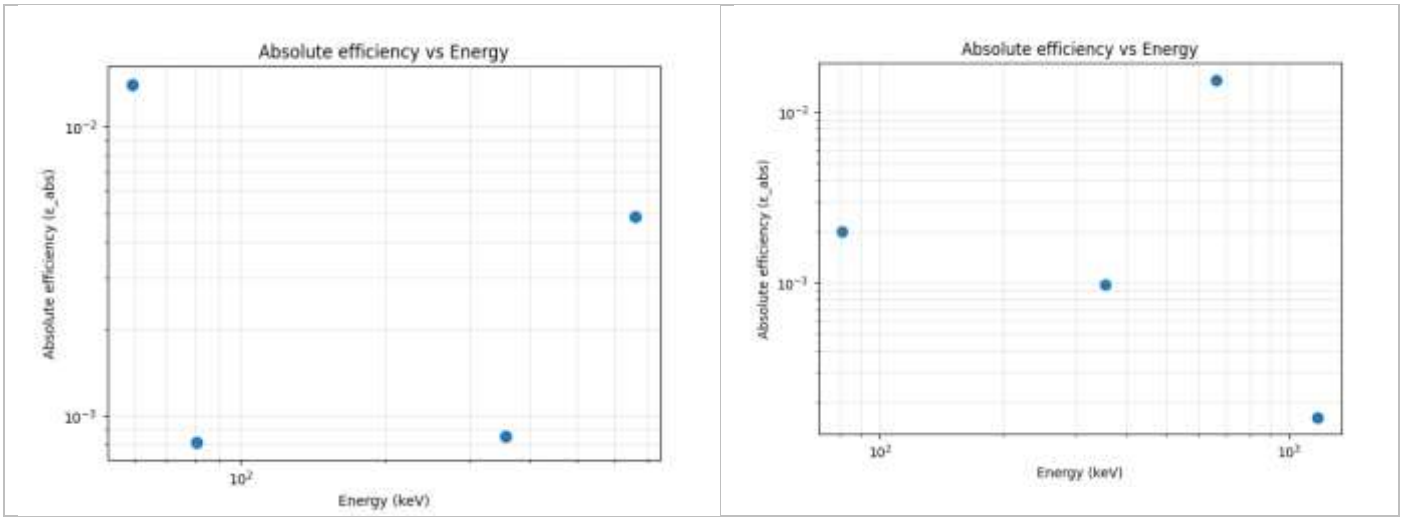

Appen Figure 11. Plotted Outputs for Absolute Efficiency.

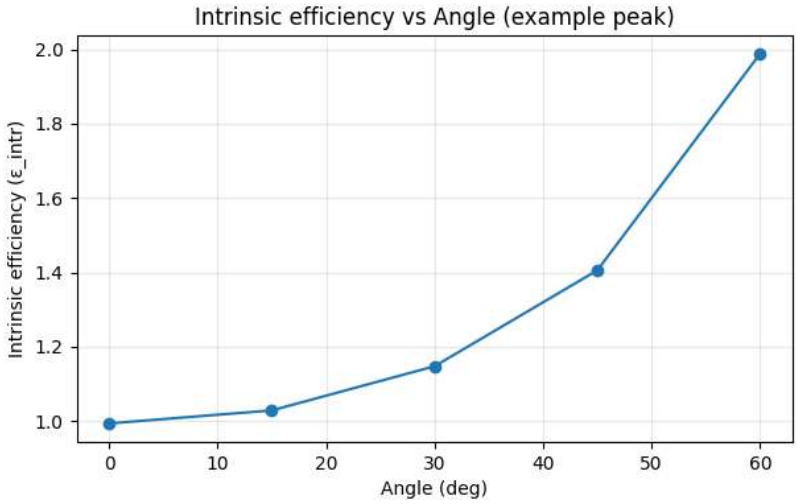

Appen Figure 12. Example Plotted Output for Intrinsic Efficiency.